NEAR-WALL VORTICITY DYNAMICS IN TURBULENT COMPRESSIBLE FLOWS

Liang Wei
Department of Mechanical and Materials Engineering
Queen's University, Kingston, Ontario
Canada K7L 3N6
email: liang@me.queensu.ca

Andrew Pollard
Department of Mechanical and Materials Engineering
Queen's University, Kingston, Ontario
Canada K7L 3N6
email: pollard@me.queensu.ca

ABSTRACT

Neal-wall vorticity dynamics in turbulent compressible channel flows are studied using direct numerical simulation (DNS). The Mach numbers of the three DNS cases are $Ma =$ 0.2, 0.7, and 1.5 respectively. The Reynolds numbers of three cases are ≈ 2800, based on the bulk velocity and the half channel width. The cross-correlation between density and spanwise vorticity is high at $y^+ \approx 4$, which is coincident with the peak mean spanwise baroclinicity. The transport equation for the mean product of density and vorticity fluctuations $\langle \rho' \omega_i' \rangle$ is presented and the distributions of terms in the $\langle \rho' \omega_z' \rangle$ transport equation indicate that the minima and maxima of the profiles are located around $y^+ \approx 5$. The relationship between pressure gradients and vorticity fluxes for compressible turbulent flows with variable viscosity has been analyzed quantitatively. Some correlations between pressure gradient and vorticity flux are found high very near the wall. The correlation are affected by Mach number and viscosity in this region.

1 Introduction

Vorticity can be generated at a solid wall, and/or through the cross product of density gradient and pressure gradient, which is referred to as baroclinic torque or baroclinicity. There are many quantities, such as pressure gradients, fluid properties, Mach number, etc that can influence the evolution of vorticity. Previous studies on vorticity dynamics include the linkage between pressure gradient and vorticity generation on a solid wall in laminar and turbulent flows; however, few studies exist for the pressure, density and vorticity interactions, as well as quantitatively evaluating the linkage between pressure gradient and vorticity generation as a function of Mach number and wall-normal distance. Clarifying the interactions among pressure, density, vorticity and their gradients is of great importance to understand the mechanism of vorticity evolution in wall bounded compressible turbulent flows.

The influence of pressure gradients and fluid properties on vorticity flux has been considered by a number of researchers, see Lighthill (1963), Wu *et al.* (1988), Gad-El-Hak (1990), Wu *et al.* (1993). Developments of boundary vorticity dynamics theory were reviewed by Wu & Wu (1998). The interaction between pressure gradients and vorticity flux was employed in flow control (Koumoutsakos, 1999; Lee & Kim, 2002). The previous studies have considered the interplay between pressure gradient and vorticity flux applied to incompressible flow; the relationship between them has been considered neither for compressible flow as a function of distance from a solid wall nor for the case when the viscosity is spatially variable. The motivation for the current study is therefore to explore the variation in the correlations of the pressure gradients and vorticity flux in near wall turbulent flows as a function of Mach number for a constant wall temperature, and to study the interactions among pressure, density, and vorticity in compressible wall bounded turbulent flows.

2 Vorticity dynamics in turbulent compressible channel flow

DNS of fully developed compressible turbulent flow between two isothermal parallel plates at three different Mach numbers was carried out using a discontinuous Galerkin method (Karniadakis & Sherwin, 2005). The Mach numbers of the cases considered were $Ma = 0.2$, $Ma = 0.7$, and $Ma = 1.5$ respectively, referred to as Ma02, Ma07, and Ma15 hereafter. The Mach number is defined as $Ma = U_m/\sqrt{\gamma R T_w}$, where U_m was the mean bulk velocity and T_w the wall temperature ($T_w = 293.15K$ for all three cases). The Reynolds number was ≈ 2800 in all cases, based on U_m, h (half channel width), the mean bulk density ρ_m, and the dynamic viscosity at the wall μ_w. The flow was assumed to be periodic in the streamwise and spanwise directions. An analysis of

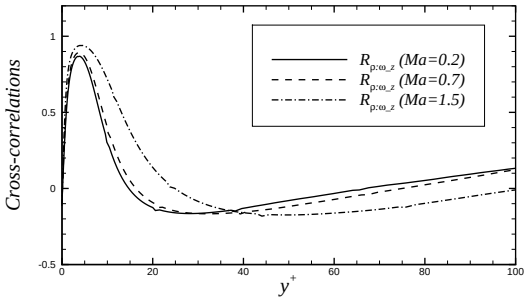

Figure 1. Cross-correlation coefficients between density (ρ) and spanwise vorticity (ω_z) close to the bottom wall in wall units.

the Kolmogorov microscale, one dimensional energy spectra and correlations showed that the grid resolution was fine enough to capture the smallest scales and the domain size was large enough to include the largest eddies in the flow, see Wei (2009). The current simulation results including mean profiles, second-order and higher-order statistics was compared with the incompressible DNS data of Moser *et al.* (1999) and compressible DNS data of Coleman *et al.* (1995), see Wei (2009) and Wei & Pollard (2011) for details. Very good agreement was found between the current simulations and the two reference cases.

2.1 Interactions among pressure, density and vorticity

The interaction between pressure, density, and vorticity is explored using cross-correlations. The cross-correlation coefficient (between variable a and variable b) is defined as: $R_{a:b} = \langle a^{'} b^{'} \rangle / \langle a^{'} a^{'} \rangle^{0.5} \langle b^{'} b^{'} \rangle^{0.5}$ where angle brackets ($\langle\ \rangle$) denotes the mean value, averaged over time and $x-z$ directions and the apostrophe($'$) denotes fluctuations with respect to the mean.

Pressure and density are perfectly correlated on the wall since the temperature fluctuations are zero on the isothermal wall. The correlation between pressure and every component of the vorticity is found to be negligible; however, there is a significant correlation between density and spanwise vorticity close to the bottom wall for all three cases Ma02, Ma07 and Ma15, see figure 1. It indicates that the maximum correlation occurs around $y^+ \approx 4$ for all cases (there is a very slight shift away from the wall with increasing Mach number). The peak correlation coefficients are around 0.9 and they increase (mildly) with Mach number. In other words, compressible isothermal-wall channel flows share a common feature that density and spanwise vorticity are highly correlated at $y^+ \approx 4$.

To explore the spatial distribution of density and spanwise vorticity around $y^+ = 4$, snapshots of density and spanwise vorticity contours at $y^+ \approx 1, 4, 20$ for the case Ma15 are given in figure 2. In the figure, the blue and gray shades represent positive and negative fluctuations respectively about a mean value. At $y^+ \approx 4$, the density (figure 2b), and the spanwise vorticity (figure 2e) share similar long regions of streamwise streaks in both size and position, which further confirms their high correlation around this location. However the density and spanwise vorticity behave differently at $y^+ \approx 1$ and $y^+ \approx 20$. The spanwise vorticity streaks at $y^+ \approx 1$ (figure 2d) look very similar with those at $y^+ \approx 4$ (figure 2e), which is different in shape and size from those streaks at $y^+ \approx 20$ (figure 2f). The spanwise vorticity is defined as $\omega_z = -\partial u/\partial y + \partial v/\partial x$, where $-\partial u/\partial y$ is the dominant term and $\partial v/\partial x$ is negligible within the viscous sublayer $y^+ < 5$. The streaks of the spanwise vorticity should be similar as those of the streamwise velocity in this viscosity-dominant region. Away from the wall, the spanwise vorticity streaks become less coherent and organized with decreasing viscous effects and increasing turbulence activity.

Unlike the spanwise vorticity, the density streaks change considerably within the viscous sublayer, but the change between $y^+ \approx 4$ and $y^+ \approx 20$ is small, see figures 2a, 2b, and 2c. The main reason is that temperature has a significant influence on density through the equation of state including the influence of the isothermal wall. On the isothermal wall, the temperature fluctuations are zero and density and pressure are non-zero and are perfectly correlated. The influence of temperature fluctuations on the density streaks is negligible. Away from the wall, temperature fluctuations increase in magnitude and play an increasingly important role on the density fluctuations. Note that temperature streaks are coherent close to the wall, as shown in figure 3. The streamwise coherence of density streaks is increased from $y^+ \approx 1$ to $y^+ \approx 4$. Although density and spanwise vorticity develop differently with distance from the wall, they are well correlated at $y^+ \approx 4$, as noted in figure 1.

The mean spanwise component of the baroclinic vector ($\langle\beta_3\rangle$ or $\langle\beta\_z\rangle$), nondimensionalized by U_m^2/h^2, for three cases is displayed in figure 4. Note that the profiles for the cases Ma02 and Ma07 are almost identical. The locations of the peak values are the same as the correlation in figure 1, although the magnitude of the peak for Ma15 is markedly higher than the others. The trend of the curves is similar and the intersection between the profile for the case Ma15 and those for the cases Ma02/Ma07 is located approximately at $y^+ \approx 40$ in both figures. The cross correlations between $\langle\beta_3\rangle$ and $\langle\rho^{'}\omega_3^{'}\rangle$ have shown that although the magnitudes of the correlation coefficients are not high very close to the wall, peaks in the profiles are located at $y^+ \approx 3-4$.

To investigate why the peak values of the correlation occur at $y^+ \approx 4$ instead of on the wall or some other regions, the transport equation for $\langle\rho^{'}\omega_i^{'}\rangle$ is derived. Through Reynolds averaging and some algebraic manipulation of the vorticity equation, it is

$$\overbrace{\frac{\partial\langle\rho^{'}\omega_i^{'}\rangle\langle u_j\rangle}{\partial x_j}}^{A} = -\overbrace{\frac{\partial\langle\rho^{'}\omega_i^{'}u_j^{'}\rangle + \langle\rho^{'}u_j^{'}\rangle\langle\omega_i\rangle}{\partial x_j}}^{D} + \overbrace{\langle\rho^{'}(\omega_j\frac{\partial u_i}{\partial x_j})^{'}\rangle}^{S} \underbrace{-\langle\omega_i u_j\rangle\frac{\partial\langle\rho\rangle}{\partial x_j}}_{G} \underbrace{-\langle\rho\omega_i\frac{\partial u_j}{\partial x_j}\rangle}_{d} + \underbrace{\langle\rho^{'}\beta_i^{'}\rangle}_{B} + \underbrace{\langle\rho^{'}\eta_i^{'}\rangle}_{V} . \quad (1)$$

The first term on the left-hand side of equation 1 is the advection term (A). The first term on the right-hand side of

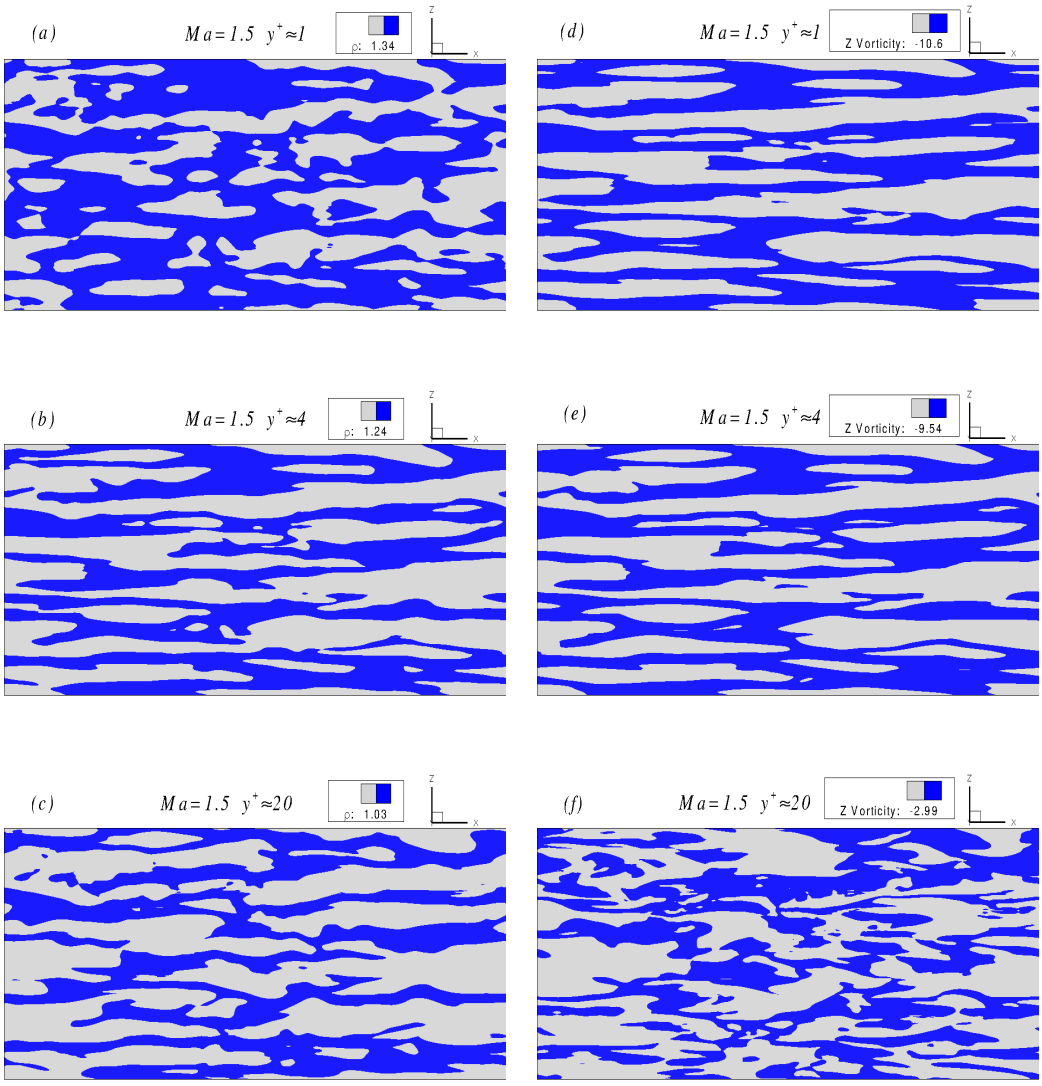

Figure 2. Contours of density and spanwise vorticity, nondimensionalized by ρ_m and U_m/h respectively, on $(x-z)$ planes close to the wall for the case Ma15. (a) Density at $y^+ \approx 1$; (b) Density at $y^+ \approx 4$; (c) Density at $y^+ \approx 20$; (d) Spanwise vorticity at $y^+ \approx 1$; (e) Spanwise vorticity at $y^+ \approx 4$; (f) Spanwise vorticity at $y^+ \approx 20$. Threshold is taken as the mean value at the respective y location so that the blue colour represents the positive fluctuations with respect to the mean and the gray colour negative.

equation 1 is the diffusion term (D). The second term (S) denotes the stretching of vorticity. The third term (G) represents the contributions from the gradients of density. The fourth term (d) is the dilatation term. The fifth term (B) is involved with baroclinicity and density fluctuations. The sixth term (V) denotes the influence of viscous effects. The distribution of these terms is shown in figure 5. A and B are essentially zero for all three cases.

For Ma02, shown in figure 5a, the two dominant terms are d and V. One might wonder why the term d is dominant as the local mean dilatation is almost negligible for Ma02. The main reason is that the term d also includes the dilatation related fluctuation terms which clearly must balance V simply because all other terms in equation 1 (D, S, and G) are found to be nearly zero. The peaks in these curves occur at about $y^+ \approx 4$. For Ma07, shown in figure 5b, d follows the trend and magnitudes established at Ma02. However, V decreases in magnitude at the expense of growth in other terms (D, S, and G) in the transport equation. The interesting feature of figure 5b is the viscous term. It displays the beginning of a transition from a simple decay process from $y^+ \approx 4$ to $y^+ \approx 20$ at Ma02 to one where the maximum is shifted farther away from the wall with a concomitant inflexion at $y^+ \approx 2$. The trends established at Ma07 are further enhanced in the case of Ma15, shown in figure 5c. The maximum negative value for the dilatation has moved slightly farther away form the wall to $y^+ \approx 6$. The vortex stretching term, S now dominates and is assisted by increased diffusion (D) and transportation through density gradient (G).

The peak locations of the profiles of D, S and G change

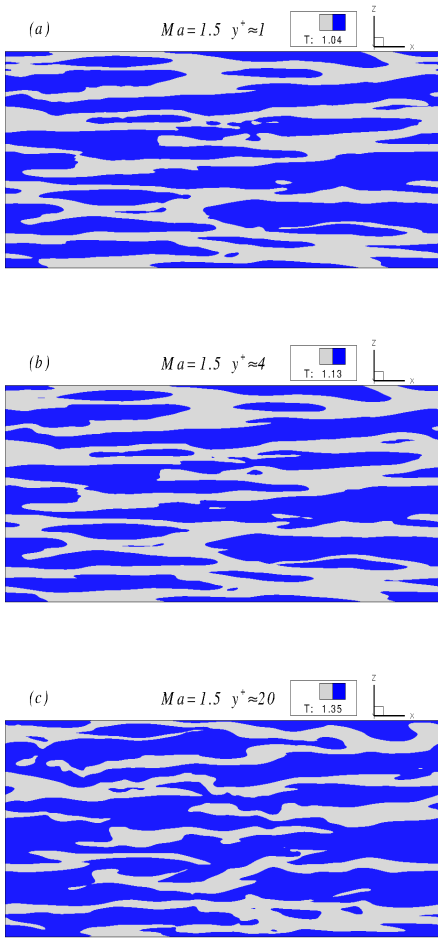

Figure 3. Contours of temperature, nondimensionalized by the wall temperature T_w, on $(x-z)$ planes close to the wall for the case Ma15. (a) $y^+ \approx 1$; (b) $y^+ \approx 4$; (c) $y^+ \approx 20$. Threshold is taken as the mean value at the respective y location so that the blue colour represents the positive fluctuations with respect to the mean and the gray colour negative.

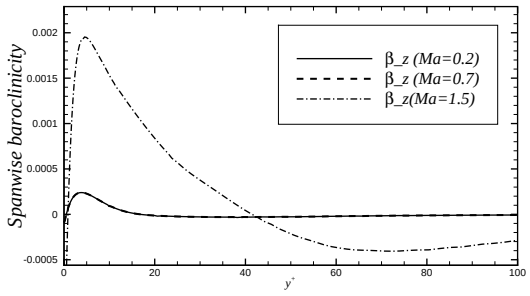

Figure 4. Mean spanwise component of the baroclinic vector (β_z) nondimensionalized by the bulk velocity and half channel width close to the wall in wall units.

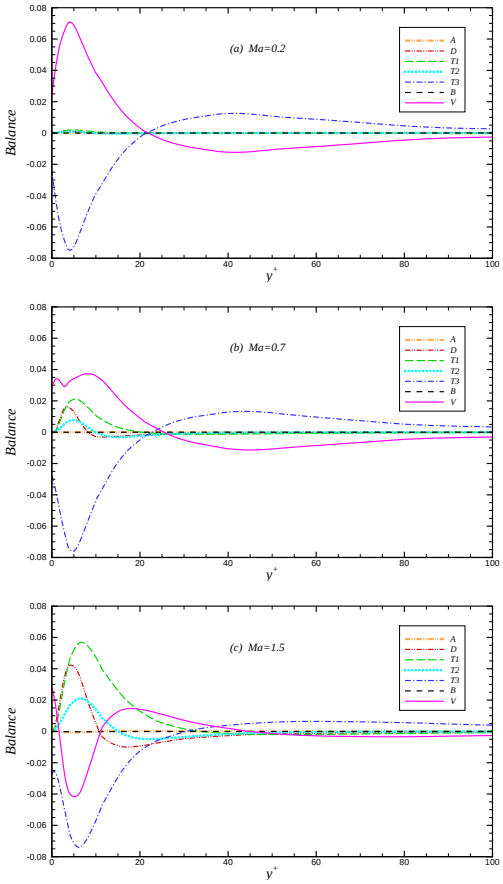

Figure 5. Balance of $\rho' \omega_i'$: (a) Ma=0.2; (b) Ma=0.7; (c) Ma=1.5. A denotes $\partial\langle\rho'\omega_i'\rangle\langle u_j\rangle/\partial x_j$; D denotes $-\partial(\langle\rho'\omega_i'u_j'\rangle + \langle\rho' u_j'\rangle\langle\omega_i\rangle)/\partial x_j$; $T1$ denotes $\langle\rho'(\omega_j \partial u_i/\partial x_j)'\rangle$; $T2$ denotes $-\langle\omega_i u_j\rangle\partial\langle\rho\rangle/\partial x_j$; $T3$ denotes $-\langle\rho\omega_i\partial u_j/\partial x_j\rangle$; B denotes $\langle\rho'\beta_i'\rangle$; V denotes $\langle\rho'\eta_i'\rangle$; where $i=3$ and $j=1,2,3$.

little as Mach number increases. Conversely, V close to the wall drops significantly when Mach number increases, due to the combined effect of viscosity and shear. The value of V on the wall, however, remains almost constant with Mach number. Note that the wall temperature and its fluctuation remain the same for all three cases, so do the viscosity and its fluctuation on the wall. For all profiles with peaks/minimums, the locations of these peaks/minimums are around $y^+ \approx 5$, which in some sense suggests this active region around the edge of viscous sublayer where the peaks of the correlation between the density and the spanwise vorticity are located.

2.2 Pressure gradient and vorticity flux

For compressible flows, the momentum equation can be written as (no assumption has been made about the spatial variation of viscosity):

$$\rho\frac{\partial u_i}{\partial t}+\rho u_j\frac{\partial u_i}{\partial x_j}+\frac{\partial p}{\partial x_i}=-\mu\varepsilon_{ijk}\frac{\partial \omega_k}{\partial x_j}+\frac{4}{3}\mu\frac{\partial \Theta}{\partial x_i}+\frac{\tau_{ij}}{\mu}\frac{\partial \mu}{\partial x_j}+\rho f_i\,, \tag{2}$$

where Θ denotes the dilatation $\Theta = \partial u_j/\partial x_j$.

After some arrangements, the relation between pressure gradient and vorticity flux on an isothermal wall is derived:

$$\frac{\partial p}{\partial x} = -\mu\frac{\partial \omega_z}{\partial y} + \frac{\partial u}{\partial y}\frac{\partial \mu}{\partial y} + \frac{4}{3}\mu\frac{\partial \Theta}{\partial x} + \rho f_x \,, \quad (3)$$

$$\frac{\partial p}{\partial y} = -\mu\frac{\partial \omega_x}{\partial z} + \mu\frac{\partial \omega_z}{\partial x} + \frac{4}{3}\mu\frac{\partial \Theta}{\partial y} + \frac{4}{3}\Theta\frac{\partial \mu}{\partial y} \,, \quad (4)$$

$$\frac{\partial p}{\partial z} = \mu\frac{\partial \omega_x}{\partial y} + \frac{\partial w}{\partial y}\frac{\partial \mu}{\partial y} + \frac{4}{3}\mu\frac{\partial \Theta}{\partial z} \,. \quad (5)$$

Further refinement of equations 3, 4, 5 gives,

$$\frac{\partial p}{\partial x} = -\frac{\partial \mu\omega_z}{\partial y} + \frac{4}{3}\frac{\partial \mu\Theta}{\partial x} + \rho f_x \,, \quad (6)$$

$$\frac{\partial p}{\partial y} = -\frac{\partial \mu\omega_x}{\partial z} + \frac{\partial \mu\omega_z}{\partial x} + \frac{4}{3}\frac{\partial \mu\Theta}{\partial y} \,, \quad (7)$$

$$\frac{\partial p}{\partial z} = \frac{\partial \mu\omega_x}{\partial y} + \frac{4}{3}\frac{\partial \mu\Theta}{\partial z} \,. \quad (8)$$

The cross-correlations between pressure gradients and vorticity fluxes have not been investigated. $R_{\partial p/\partial x_k:\partial\mu\omega_i/\partial x_j}$ and $R_{\partial p/\partial x_k:\partial\omega_i/\partial x_j}$ for three cases (Ma02, Ma07, and Ma15) were generated to investigate the influence of Mach number, viscosity, and compressibility/dilatation. Of the 54 correlations considered in $R_{\partial p/\partial x_k:\partial\mu\omega_i/\partial x_j}$ and $R_{\partial p/\partial x_k:\partial\omega_i/\partial x_j}$, only 6 were found to be significant. Additionally, cross-correlations $R_{p:\partial\omega_i/\partial x_j}$ and $R_{\partial p/\partial x_k:\omega_i}$ were also generated; however, all these correlations were found to be very small and thus are not be shown here. Therefore, only the highly correlated terms within $R_{\partial p/\partial x_k:\partial\mu\omega_i/\partial x_j}$ and $R_{\partial p/\partial x_k:\partial\omega_i/\partial x_j}$ are discussed in the following sections.

The cross-correlation coefficients between streamwise pressure gradient and spanwise vorticity flux in the wall-normal direction $R_{\partial p/\partial x:\partial\mu\omega_z/\partial y}$ and $R_{\partial p/\partial x:\partial\omega_z/\partial y}$ are shown in figure 6. The absolute value of the correlation coefficients decreases as Mach number increases because of the influence of ρf_x in which the density fluctuation increases with increasing Mach number. The profile of $R_{\partial p/\partial x:\partial\mu\omega_z/\partial y}$ for three cases scales well with Mach number in the region $0.5 < y^+ < 5$. The difference between two correlations $R_{\partial p/\partial x:\partial\mu\omega_z/\partial y}$ and $R_{\partial p/\partial x:\partial\omega_z/\partial y}$ on the wall is negligible except for $0 < y^+ < 4$, where there is a clear departure of $R_{\partial p/\partial x:\partial\omega_z/\partial y}$ from its viscosity related correlation for the case Ma15 and it is to this that attention is now turned.

The fluctuation of temperature is zero on the isothermal wall and wall-normal gradient of the temperature fluctuation on the wall is very small for the cases considered here. As viscosity is a function of temperature only, both the fluctuation of viscosity and its wall-normal gradient are negligible on the wall, so that the direct influence of the viscosity μ on the correlation $R_{\partial p/\partial x:\partial\mu\omega_z/\partial y}$ is negligible on the wall for the current cases. The difference will probably not be negligible if Mach number is much higher than the current cases. Very close to the wall, however, the fluctuations of temperature and

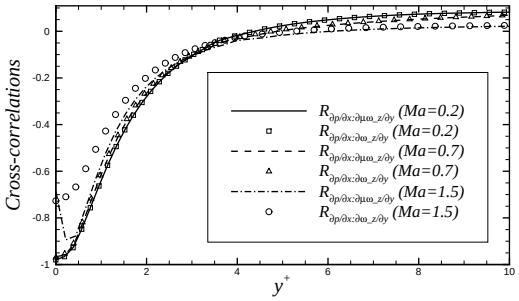

Figure 6. Cross-correlation coefficients between streamwise pressure gradient and spanwise vorticity fluxes in the wall-normal direction including the influence of viscosity.

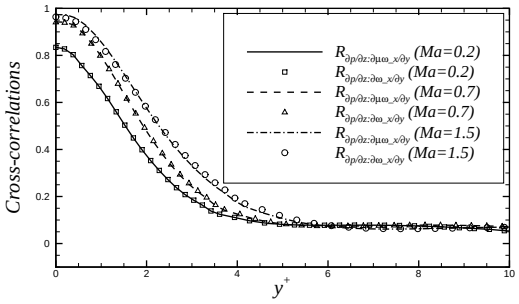

Figure 7. Cross-correlation coefficients between spanwise pressure gradient and streamwise vorticity fluxes in the wall-normal direction including the influence of viscosity.

viscosity as well as their wall-normal gradients increase significantly as Mach number increases from subsonic to supersonic, which is the main reason for the difference of the two profiles very close to the wall for the case Ma15.

The cross-correlation coefficients between spanwise pressure gradient and streamwise vorticity flux in the wall-normal direction $R_{\partial p/\partial z:\partial\mu\omega_x/\partial y}$ and $R_{\partial p/\partial z:\partial\omega_x/\partial y}$ are presented in figure 7. High positive correlation coefficients are observed close to the wall. Unlike figure 6, the absolute values of correlation coefficients in figure 7 approach 1.0 as the Mach number increases. The profile of $R_{\partial p/\partial z:\partial\mu\omega_x/\partial y}$ for three cases does not scale with Mach number very close to the wall. It seems that the term $\partial\mu\Theta/\partial z$, compared with the terms $\partial p/\partial z$ and $\partial\mu\omega_x/\partial y$ in equation 8, becomes relatively less important on the wall as Mach number increases. The difference between the correlations $R_{\partial p/\partial z:\partial\mu\omega_x/\partial y}$ and $R_{\partial p/\partial z:\partial\omega_x/\partial y}$ is almost negligible for the current cases; but the trend suggests that the difference increases slightly with increasing Mach number. Compared with the difference for the case $Ma = 1.5$ observed in figure 6, the difference for the $Ma = 1.5$ in figure 7 is negligible and this is because $\partial w/\partial y < \partial u/\partial y$ very near the wall.

The cross-correlation coefficients between wall-normal pressure gradient and streamwise vorticity flux in the spanwise direction $R_{\partial p/\partial y:\partial\mu\omega_x/\partial z}$ and $R_{\partial p/\partial z:\partial\omega_x/\partial z}$ are given in figure 8. It is evident that there is little difference between

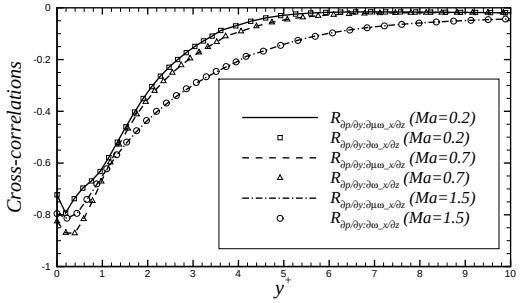

Figure 8. Cross-correlation coefficients between wall-normal pressure gradient and streamwise vorticity fluxes in the spanwise direction including the influence of viscosity.

these correlations. This is obvious because the term $\partial\mu\omega_x/\partial z$ in equation 7 is equal to the term $\mu\partial\omega_x/\partial z$ in equation 4. The correlation coefficients for all three cases are also high on the wall. The profile of $R_{\partial p/\partial y:\partial\mu\omega_x/\partial z}$ for three cases does not collapse with Mach number very close to wall. However, it is interesting to note that the highest correlation occurs for the case Ma07 and the profile for the case Ma15 in the region around the edge of viscous sublayer is higher than the other two cases, which could be due to the combined effects of wall-normal gradients of viscosity, dilatation, and advection. The wall-normal pressure gradient correlation shows a more complicated behaviour than the wall-tangential pressure gradient correlations. In addition, the term $\partial\mu\omega_z/\partial x$ in equation 7 is not well correlated with $\partial p/\partial y$ on the wall because $\partial\mu\omega_z/\partial x$ is much smaller than $\partial\mu\omega_x/\partial z$ there. The driving force in the streamwise direction leads to large streamwise shear stress close to the wall, which causes streaks and vortex lines close to the wall to be stretched in the streamwise direction. This streamwise stretching makes streamwise gradients smaller than spanwise gradients.

It is also interesting to note from the above figures that high correlations between pressure gradients and vorticity fluxes only exist very close to the wall. The correlations are almost negligible in the region removed from the viscous sublayer. As equation 2 suggests, the vorticity flux is also affected by advection, besides viscosity and pressure gradients. The advection is negligible very close to the wall and viscosity effects dominate; however, advection begins to play a dominant role away from the wall. Advection is an important reason that the high correlation between pressure gradient and vorticity flux decreases with distance from the wall. In other words, when the vorticity is generated on the wall, the pressure gradient plays an important role as advection very near the wall is small. The vorticity is then diffused into the flow first due to viscosity before being advected away.

3 Summary

The near-wall vorticity dynamics in turbulent compressible flows are studied using DNS. DNS of three isothermal-wall turbulent channel flows for Mach number $Ma = 0.2$, 0.7, and 1.5 respectively are performed using DGM. The Reynolds numbers of three cases are ≈ 2800. A high cross-correlation between density and spanwise vorticity occurs at $y^+ \approx 4$, which is coincident with the peak mean spanwise baroclinicity. The difference between the evolution of density and spanwise vorticity very near the wall is discussed. The transport equation for the mean product of density and vorticity fluctuations $\langle\rho'\omega_i'\rangle$ is presented. The connection between pressure gradients and vorticity fluxes for compressible turbulent flows with variable viscosity has been formulated and verified. High correlations $(0.7-1.0)$ between pressure gradient and vorticity flux are found very close to the wall ($y^+ < 5$). The correlation coefficients are significantly influenced by *Ma* and viscosity in this region.

Acknowledgments

The authors would like to thank Dr. George Karniadakis & his CRUNCH group and Dr. Mike Kirby for providing the original discontinuous Galerkin code and the related helpful email discussions. The research was funded through grants from NSERC Canada. Computing resources were provided by HPCVL (www.hpcvl.org).

REFERENCES

Coleman, G. N., Kim, J. & Moser, R. D. 1995 A numerical study of turbulent supersonic isothermal-wall channel flow. *J. Fluid Mech* **305**, 159–183.

Gad-El-Hak, M. 1990 Control of low-speed airfoil aerodynamics. *AIAA Journal* **28** (9), 1537–1552.

Karniadakis, G.E. & Sherwin, S. 2005 *Spectral/hp Element Methods for Computational Fluid Dynamics*, 2nd edn. Oxford Science Publications.

Koumoutsakos, P. 1999 vorticity flux control for a turbulent channel flow. *Phys. Fluids* **11** (2), 248–250.

Lee, C. & Kim, J. 2002 Control of viscous sublayer for drag reduction. *Phys. Fluids* **14** (7), 2523–2529.

Lighthill, M. J. 1963 *Introduction. Boundary Layer Theory, chapter II in Laminar Boundary Layers*. Oxford University Press.

Moser, R. D., Kim, J. & Mansour, N. N. 1999 Direct numerical simulation of turbulent channel flow up to $Re_\tau \approx 590$. *Phys. Fluids* **11** (4), 943–945.

Wei, L. 2009 Direct numerical simulation of compressible and incompressible wall bounded turbulent flows with pressure gradients. PhD thesis, Queen's University, Kingston, Ontario, Canada.

Wei, L. & Pollard, A. 2011 Direct numerical simulation of compressible turbulent channel flows using the discontinuous Galerkin method. *Comput. Fluids* DOI:10.1016/j.compfluid.2011.02.015.

Wu, J. Z. & Wu, J. M. 1998 Boundary vorticity dynamics since Lighthill's 1963 article: review and development. *Theoret. Comput. Fluid Dynamics* **10**, 459–474.

Wu, J. Z., Wu, J. M. & Wu, C. J. 1988 A viscous compressible flow theory on the interaction between moving bodies and flow field in the $(\omega,\ \vartheta)$ framework. *Fluid Dynamics Research* **3**, 203–208.

Wu, J. Z., Wu, X. H. & Wu, J. M. 1993 Streaming vorticity flux from oscillating walls with finite amplitude. *Phys. Fluids A* **5**, 1933–1938.